Spatial resets modulate YAP-dependent transcription

*****J. Matthew Franklin[1-5], *****Rajarshi P. Ghosh[1-4], Quanming Shi[1-4], [#]Jan T. Liphardt[1-4]

[1] Bioengineering, Stanford University, Stanford, CA 94305, USA
[2] BioX Institute, Stanford University, Stanford, CA 94305, USA
[3] ChEM-H, Stanford University, Stanford, CA 94305, USA
[4] Cell Biology Division, Stanford Cancer Institute, Stanford, CA 94305, USA
[5] Chemical Engineering, Stanford University, Stanford, CA 94305, USA

***** Authors contributed equally.
[#] Correspondence and requests for materials should be addressed to jan.liphardt@stanford.edu

Yes Associated Protein 1 (YAP), an integral component of the Hippo pathway, plays critical roles in mechanotransduction, organ size control, and regeneration. Using live imaging of CRISPR-knockin cell lines, we show that endogenous YAP undergoes concerted fluctuations between the nucleus and the cytoplasm in diverse signaling contexts. Additionally, using nascent-transcription reporter knockins we show that these spatiotemporal YAP oscillations are strongly correlated to transcriptional outputs from endogenous YAP targets. Maximal transcriptional responses are preceded by a spatial 'reset' characterized by bulk exit of YAP from the nucleus followed by re-entry. Transcriptional enhancement through spatial reset of YAP could be achieved by targeting Src-kinase, releasing store-operated Ca^{2+}, and cell division. Transformed cells exhibiting much higher import and export rates of YAP and diminished interaction with bulk chromatin lacked spatial resets, pointing to an escape from compartmentalization based control of target gene expression.

Introduction

The temporal complexity of signaling networks arises through parallel activation of different signaling modules (*1*). Mediators of cellular signaling that shuttle between cellular compartments, often encode signaling cues in the form of amplitude, frequency, and duration of response (*2*)(*3*). Several transcription factors (TFs) such as NF-kB and P53, have been shown to encode upstream signaling events in the temporal patterns of their shuttling (*3-5*).

A prime example of a signal integrator that shows differential compartmentalization in response to various physiological cues is the YAP (YES-associated protein) / TAZ (transcriptional coactivator with PDZ-binding motif) duo (*6*)(*7*). In addition to the canonical Hippo pathway (*8*)(*9*), several non-canonical pathways including mechanotransduction (*10*), 3D architectural reorganization (*11*) and cellular crowd sensing (*12*) have been shown to converge on the YAP/TAZ response module. The classic view of YAP equates high expression and nuclear enrichment with downstream activation of pro-growth transcriptional programs (*9*)(*13*), primarily through association with TEAD (*14-17*). Dysregulated YAP signaling has been implicated in several forms of cancer, although several conflicting views exist (*9*), pointing to a gap in the mechanistic understanding of the role of YAP in oncogenic transformation.

Recent works have aimed at delineating the mechanistic basis of YAP shuttling using live imaging of ectopically expressed YAP in mammalian cells (*18*)(*19*) or native YAP in *D. Melanogaster* (*20*). While there is mounting evidence that YAP signaling is highly dynamic, a comprehensive understanding of the relationship between YAP localization and transcriptional control is missing. A recent study demonstrated that a “biphasic switch” in YAP localization upon treatment with Angiotensin II was required for activating YAP responsive genes (*21*). This study raises the intriguing possibility that YAP dependent transcription is not a simple linear function of the cumulative nuclear abundance of YAP (*21*).

Here we perform a dynamical analysis of the relationship between YAP and its target genes, using real-time tracking of both YAP localization dynamics and nascent transcription dynamics of endogenous YAP responsive alleles. To track YAP and TEAD in real time, we used CRISPR to fluorescently tag the native genes in breast epithelial cell lines (*22*)(*23*), to keep the natural feedback circuit involving YAP expression, localization and cellular signaling intact. Since gene transcription is pulsatile in nature (*24-26*), defining the relationship between YAP localization and target gene activity would require continuously tracking the transcriptional state of YAP target genes. To track potential fluctuations in YAP dependent transcription, we tagged native mRNA of two well documented YAP target genes, ANKRD1 (*27*) and AREG (*28*), with a 24X MS2 transcriptional reporter cassette using CRISPR.

We have identified fluctuations in YAP localization that are modulated by a variety of input-parameters including oncogenic transformation, calcium signaling, acto-myosin contractility, and mitotic exit. Pharmacological induction of store operated Ca 2+ entry (SOCE) induced marked nuclear deformation and concomitant YAP spatial-reset, which was substantially diminished in cells with defective nuclear lamina or impaired LATS kinase activity. Real-time tracking of nascent transcription of ANKRD1 and AREG genes revealed that transient YAP spatial-resets induced by calcium, SRC inhibition, and mitosis were correlated with rapid transcriptional activation of YAP target genes. Ras transformation of mammary epithelial cells, which promotes YAP target gene expression, increased nucleocytoplasmic turnover of YAP,

reduced bulk chromatin binding, and dampened fluctuations in global YAP localization. These results suggest a model of transcriptional activation gated by YAP nuclear retention, which is bypassed by Ras transformation.

Results and Discussion

Genome knockin lines reveal endogenous YAP and TEAD dynamics

The current model of transcriptional control through differential localization of YAP is based on bulk cellular assays. Our initial goals were (i) to track the dynamic changes in native YAP localization across a broad range of timescales in response to different signaling cues and (ii) to determine the relationship between YAP localization and transcriptional dynamics of YAP target genes.

Using CRISPR/Cas9 assisted target gene editing, we generated a C-terminal eGFP fusion of native YAP (Methods, Figure 1a) in the MCF10A breast epithelial cell line and the HRas transformed version, MCF10AT (*29*) (Figure 1b). Confocal images of these cell lines at different monolayer densities confirmed previously observed density-dependent cytoplasmic sequestration of YAP in MCF10A (*13*) (Figure 1b, upper panel), whereas in MCF10AT this distinction was minimal (Figure 1b, lower panel). To construct a time-resolved view of density-sensing by YAP, we simultaneously tracked local cell density (Methods) and YAP localization in a 2D monolayer over multiple days. In MCF10A$^{\text{YAP-GFP-KI}}$ cells, we observed a global shift in the nuclear-to-cytoplasmic ratio (N/C) over time (Figure 1c, Supplementary Movie 1). Plotting N/C and neighborhood-density over time revealed that the monolayer maintains both constant YAP N/C and local cellular density until a sensing threshold is met, after which N/C decreases sharply with a concomitant increase in local cell density (Figure 1c). This suggests that at low density, newly divided cells can migrate to void-spaces to maintain a constant local cell density. Further division cycles deplete the voids, forcing cells to pack and thereby activating the *Hippo* pathway and consequent cytoplasmic sequestration of YAP.

In contrast, we found that HRas transformed MCF10A cells (MCF10AT $^{\text{YAP-GFP-KI}}$) (*29*) did not show cytoplasmic sequestration at high density (Figure 1d, Supplementary Movie 2). HRas transformation has been shown to decrease LATS1/2 activity (*30*)(*31*), which is the primary kinase involved in density sensing and cytoplasmic sequestration of YAP (*9*)(*12*). The diminished YAP N/C dynamic range in HRas transformed cells indicates compromised *Hippo* signaling and YAP localization control.

TEA domain transcription factors (TEAD), which are the primary nuclear interaction partners of YAP (*14*), have been shown to undergo cytoplasmic sequestration in Hek293 cells at high cell density (*32*). To simultaneously track YAP and TEAD subcellular localization in real time, we generated a dual CRISPR knockin MCF10A cell line where native YAP and TEAD1 were genomically tagged with eGFP and mCherry respectively (Methods, Figure 1e). Unlike Hek 293 cells, MCF10A$^{\text{YAP/TEAD1dual KI}}$ showed no significant cytoplasmic sequestration of TEAD1 at higher cell densities (Figure 1e, f). A remarkable feature of most MCF10A$^{\text{YAP/TEAD1dual KI}}$ nuclei were two distinct TEAD1 hotspots (Figure 1g). TEAD1-eGFP knockin cells showed the same hotspots (Figure 1h). Real time tracking of TEAD1 spots showed gradual signal enhancement through late interphase, and subsequent signal decay after mitotic exit, suggesting that the increase in intensity observed during late interphase was due to duplication of a genomically defined TEAD1 interaction hub which then partitioned into two daughter cells (Figure 1h, i; Supplementary Movie 3). Further investigation will be needed to assess the importance of these hotspots.

YAP spatial-fluctuations are modulated by various signaling cues

At the single cell level, we observed large fluctuations in YAP N/C during monolayer growth, with localization inverting within 120 minutes (Figure 2a, Supplementary Movie 4). To better characterize these spatial fluctuations, we measured YAP N/C over a 24-hour period at a 15-minute frequency. Close inspection of individual traces revealed rapid changes in YAP N/C (Figure 2b, Supplementary Movie 5).

As YAP-localization is primarily controlled through phosphorylation (*33*), we hypothesized that modulating upstream kinase activity would alter YAP N/C fluctuation dynamics. To test this, we investigated the effects of HRas transformation and Src kinase inhibition on YAP fluctuations, both of which have been shown to modulate LATS activity (*31*)(*34*)(*35*). Src inhibition in serum starved MCF10A cells has been shown to cause cytoplasmic sequestration (*36*). When cultured in complete media, we found that Src inhibition by PP1 exaggerated N/C fluctuations, while HRas transformation dampened fluctuations (Figure 2b-c, Supplementary Movie 5). We found that fluctuation frequency and amplitude were unchanged (Supplementary Figure 1), however, the fraction of cells showing at least one fluctuation increased upon PP1 treatment (0.56) and decreased upon HRas transformation (0.06) compared to untreated MCF10A cells (0.23) (Figure 2c). For most MCF10A$^{\text{YAP-GFP-KI}}$ cells, fluctuations in N/C were uncorrelated with the N/C of neighboring cells (Supplementary Movie 5). However, in rare cases we observed coordinated fluctuations in N/C in a cohort of neighboring cells (Figure 2d-e, Supplementary Movie 6). Taken together, we conclude that YAP localization fluctuations occur regularly, depend on known signaling pathways, and may either be independent or happen in sync with neighboring cells.

Intracellular calcium release induces rapid YAP spatial-reset

Fluctuations in biological systems are often considered crucial for functional and phenotypic "plasticity" (*37*). To delineate the temporal scales over which YAP localization dynamics encode large and rapid changes in environment, we investigated how YAP localization is affected upon monolayer wounding. Previous immunofluorescence data have demonstrated fast (30 minutes) nuclear relocalization of YAP at the wound edge of mammary epithelial cells (*12*). Surprisingly, real-time tracking of YAP revealed an oscillatory response: rapid nuclear accumulation in edge cells (~1 minute), followed by a depletion phase lasting ~20 minutes, and finally a slow accumulation phase (~3 hrs) (Figure 3a, Supplementary Movie 7).

A fast calcium wave (FCW) within minutes of epithelial wounding has been reported in diverse cell types, including MCF10A (*38-41*). We hypothesized that intracellular calcium release may be driving the depletion phase of the wound response. To directly assess the impact of intracellular Ca^{2+} release on YAP localization dynamics we treated sub-confluent MCF10A$^{\text{YAP-GFP-KI}}$ cells with 1μM Thapsigargin (TG), a potent ER Ca^{2+} ATPase inhibitor (*42*). Interestingly, the release of intracellular Ca^{2+} resulted in a coordinated YAP translocation cycle similar to that seen at the wound edge: an initial fast depletion-phase lasting ~25 minutes followed by a slow nuclear enrichment-phase (50 minutes) (Figure 3b, Supplementary Movie 8). To monitor Ca^{2+} dynamics we generated an MCF10A cell line stably expressing the fast kinetic

Ca^{2+} sensor GcAMP6f (Methods) (*43*). TG treatment of an MCF10A^{GcAMP6f} cell line revealed a rapid increase in intracellular Ca^{2+} matching the onset time of nuclear YAP depletion, followed by a slow decay, and then a sustained low amplitude oscillatory phase (Figure 3c, Supplementary Movie 8). Such collective Ca^{2+} oscillations have been demonstrated at monolayer wound edges (*44*).

Unexpectedly, the onset of Ca^{2+} release correlated with initial rapid decrease in nuclear volume followed by pulses of compression and relaxation corresponding to calcium oscillations (Figure 3d). This phenomenon has not been previously reported but may play important roles in biomechanical regulation of calcium signaling. A recent report suggested that general nuclear import is mechanically gated by nuclear membrane tension (*19*), suggesting that the compressed nucleus may be physically inhibiting nuclear import.

Ionomycin, a Ca^{2+} ionophore (*45*) which also increases intracellular Ca^{2+}, showed similar effects to TG (Supplementary Figure 2a). Simultaneous treatment of ionomycin and the potent phosphatase inhibitor Okadaic acid, known to inhibit protein phosphatase 1 upstream of YAP (*46*), led to a similar degree of cytoplasmic sequestration with minimal recovery, suggesting that Ca^{2+} drives temporary phosphorylation of YAP (Supplementary Figure 2a). Previous reports have shown that the release of extracellular ATP may drive FCW at epithelial wound edge (*47*). Although addition of 10mM extracellular ATP induced a similar response as TG and ionomycin, we found there was a sharp dependence on local cellular density, with sparse cells responding minimally (Supplementary Figure 2b). Trapping of YAP with the crm1 export channel blocker, leptomycin B (LMB) (*48*) completely abolished the Ca^{2+} driven YAP localization-reset, suggesting that Ca^{2+} driven exodus of nuclear YAP requires an active export machinery (Supplementary Figure 2c).

Recently, immunofluorescence imaging in glioblastoma cells by Liu *et al* showed that LATS1/2 is critical to Ca^{2+}-driven phosphorylation and cytoplasmic sequestration of YAP (*49*). As previously demonstrated, cPKC activation upstream of LATS1/2 is responsible for rapid nuclear depletion of YAP (*21*)(*49*). Treatment with the potent protein kinase C inhibitor Go6976 (*49*) resulted in a delay in onset of depletion and overall reduction in the extent of depletion (Supplementary Figure 2d, Supplementary Movie 9).

Since nuclear membrane structure has been shown to mechanically regulate YAP translocation dynamics (*50*)(*51*), we hypothesized that the Ca^{2+}-induced compression of the nucleus may be contributing to the YAP spatial reset. To reduce the compressibility of the nucleus, we over-expressed the ∆50LaminA variant which confers increased rigidity to the nucleus (*52*). Indeed, ∆50LaminA overexpression reduced the mean nuclear compression by 48% after TG treatment (Supplementary Figure 3a-b) and significantly reduced Ca^{2+}-induced YAP spatial reset, suggesting that the mechanical regulation of the nucleus can contribute to fluctuations in YAP localization (Supplementary Figure 3c, Supplementary Movies 10-11).

YAP spatial-resets are correlated with target gene activation

YAP is integral to transcriptional programs that control growth, division (*9*), and apoptosis (*53*). We hypothesized that the observed YAP spatial-resets may be altering target-gene transcription. We suspected that the transcription changes may be subtle or transient, however the kinetic aspect of transcription is not adequately described by traditional RNA detection

strategies. Synthetic reporters based on fluorescent protein (FP) expression driven by YAP-responsive promoter-arrays (10) are unsuitable for real-time tracking of transcriptional activity due to inherent delay resulting from mRNA export, translation, and FP maturation times. Moreover, site of genomic integration of a synthetic reporter construct may affect transcriptional output through position effects (*54*). To circumvent these limitations, we used CRISPR (Methods) to insert a 24X-MS2 transcriptional reporter cassette (*55*) at the 3' UTR of two well documented YAP responsive genes, Amphiregulin (AREG) (*28*) and Ankyrin Repeat Domain 1 (ANKRD1) (*27*) (Figure 4a). Co-expression of an mNeon-green (*56*) fusion of the bacteriophage MS2 coat protein (*55*) (MCP-mNeon) allowed us to quantify transcriptional output by monitoring actively transcribing loci (Figure 4b).

TG treatment, which induced YAP spatial-reset, also resulted in a marked and rapid increase the number of cells showing active transcription, for both MCF10A$^{\text{AREG-MS2-KI}}$ and MCF10A$^{\text{ANKRD1-MS2-KI}}$ cells (Figure 4c, d; Supplementary Movies 12, 13). In addition to the number of cells transcribing the genes, the amplitude of the nascent spot intensity was significantly increased after TG treatment (Supplementary Figure 4a).

We hypothesized that the YAP spatial-reset is required for increased transcriptional response. Therefore, we pre-treated cells with Go6976 before treating with TG. This pre-treatment severely attenuated the transcription response in both AREG and ANKRD1 in terms of the number of cells (Figure 5e-f) and the nascent spot intensity (Supplementary Figure 4a), suggesting the YAP spatial-reset was required for maximal transcriptional enhancement seen after treatment with TG alone.

Since treatment of sub-confluent MCF10A cells with the Src inhibitor PP1 increased YAP N/C fluctuations, we hypothesized that this may increase YAP responsive transcriptional output. Indeed, both ANKRD1 and AREG showed moderate increase in transcription following PP1 treatment (Figure 4g-h). Interestingly, PP1 treatment led to an immediate (albeit moderate) increase in the number of responsive MCF10A$^{\text{ANKRD1-MS2-KI}}$ cells, but MCF10A$^{\text{AREG-MS2-KI}}$ cells showed a more gradual increase in the number of responsive cells with the effect peaking at 5-8 hours post treatment (Figure 4g, h). Additionally, PP1 treatment of MCF10A $^{\text{ANKRD1-MS2-KI}}$ cells led to a marked increase in number of long-lived transcription pulses (Supplementary Figure 4b). This suggests that while YAP spatial-resets turn on YAP responsive genes, the extent and the specific nature of the activation may reflect gene specific regulation.

During mitosis, YAP was excluded from condensed chromosomes (Figure 4i), suggesting that a controlled spatial-reset is intrinsic to cell division. We sought to understand whether the nuclear repopulation of YAP upon mitotic exit refreshes YAP transcription activity. To detect the instantaneous transcriptional state of a YAP target gene throughout the cell cycle, we synchronized MCF10A $^{\text{ANKRD1-MS2-KI}}$ cells to G1/S phase boundary using a double thymidine block and then imaged continuously for 24 hours upon release of the block. Indeed, for both MCF10A$^{\text{ANKRD1-MS2-KI}}$ cells and MCF10A$^{\text{AREG-MS2-KI}}$ cells, the number of cells showing active transcription increased markedly over a 2-hour period following mitotic exit (Figure 4j-m; Supplementary Movies 14, 15). An overlay of time dependent variation in YAP N/C on the mitotic timeline of YAP dependent gene expression, shows a distinct minimum during mitosis due to the exclusion of YAP from condensed chromatin (Figure 4 l, m).

Enhanced nuclear retention of YAP is anti-correlated with YAP activity

The current literature suggests that YAP may play a critical role in oncogenesis (*9*). Since YAP spatial-reset events showed strong temporal correlation with YAP target gene response, we sought to understand the nature of nuclear retention in terms of nuclear import, export and binding in cells with known oncogenic transformations.

Unlike MCF10A$^{YAP\text{-}GFP\text{-}KI}$, MCF10AT, SUM159, and MDA-MB-231$^{YAP\text{-}GFP\text{-}KI}$ cell lines showed no change in YAP localization upon TG treatment (Figure 5a), suggesting that Ca^{2+} induced YAP spatial-reset is perturbed by oncogenic transformations. This is line with the dampening of baseline YAP N/C fluctuations seen in Ras transformed MCF10A cells (Figure 2b, c). However, in spite of loss of spontaneous and induced spatial reset (Figure 5a), Ras transformed MCF10A exhibits higher expression of YAP-target genes (Supplementary Figure 5) compared to MCF10A. We hypothesized that transformed cells escape the need for reset based YAP activation by maintaining YAP in a hyper active form. Since spatial resets were critical to YAP activation in 10A cells, we wondered whether the hyper active nature of YAP in Ras transformed 10A cells was due to altered transport kinetics.

To investigate this possibility, we measured the baseline nuclear-cytoplasm turnover in terms of nuclear import and export rates. To quantify YAP nuclear export and import rates, we measured rate of fluorescence recovery upon photo-bleaching of the cytoplasmic or nuclear pools of YAP respectively (Figure 5b). Interestingly, we found that all the transformed cell lines had upregulated YAP nuclear export and import rates compared to MCF10A (Figure 5c). We note that the transport rates reported here are the first-order reaction rate constants, and are independent of concentration, as opposed to a net flux measurement. MCF10A however, had the highest import to export ratio (3.9) compared to all transformed cell lines (Hras=1.7, SUM159=1.7, MDA-MB-231=1.6). The upregulated import and export rates of YAP in transformed cell lines shows that YAP rapidly equilibrates between the nucleus and cytoplasm. Using an engineered nuclear transport reporter that harbors a canonical nuclear localization signal (NLS) and a nuclear export signal (NES) (See Methods), we found that the base-line nuclear export rates across all cell lines were relatively unchanged (Figure 5c), suggesting that YAP transport rates are specifically affected by malignant transformations.

Previous work has shown that YAP has increased interactions with bulk chromatin in cancer-associated fibroblasts compared to a 'non-transformed' fibroblast line (*19*). To understand whether malignant transformation also affected DNA binding in breast epithelial cells we performed high time-resolution FRAP experiments on native YAP-GFP and fit data to either pure diffusion or diffusion-reaction models (*57*) (Figure 5d, Supplementary Figure 6, Methods). We found striking differences in the degree of YAP-chromatin interactions: ~52% of YAP molecules were effectively bound in MCF10A, whereas all transformed cell lines were best described by a pure diffusion model (i.e. negligible binding) (Supplementary Table 1). This result is unexpected because YAP-chromatin binding is anti-correlated with YAP transcriptional activity. Because spatial resets correlated with high transcription output, we hypothesized that the high-degree of YAP-chromatin binding in MCF10A may act to strictly regulate transcriptional output by decreasing nucleus-cytoplasm turnover, whereas Ras transformation obviates this mechanism.

Collectively, these results suggest that transformed cell lines escape the fine-tuned control of YAP localization seen in MCF10A cells by maintaining elevated nuclear-cytoplasmic

turnover.

Outlook

Our results suggest a new regulatory mechanism for YAP dependent transcription where ‘spatial resets’ may be central to gene activation. Using inhibitor studies and oncogenic Ras transformation, we found that LATS kinase is central to YAP spatial resets (Figure 5e). Real-time imaging of YAP target-gene transcription revealed a strict correlation to spatial resets, pointing to a transcriptional control mechanism based on differential access to cellular compartments. It has been suggested that extended nuclear retention can inhibit transcription factor activity through posttranslational modifications which can be reversed through re-localization to the cytoplasmic compartment (*58*)(*59*). Such reactivation of inactive nuclear transcription factors through transient localization to cytoplasm has been proposed for nuclear factor erythroid 2-related factor 2 (Nrf2) (*58*).

Ras transformed cells characterized by lower nuclear retention of YAP exhibit higher baseline transcription of YAP target genes compared to untransformed cells. This raises the intriguing possibility that prolonged nuclear retention deactivates YAP which is reactivated through spatial-reset cycles (Figure 5f). On the other hand, the rapid nucleocytoplasmic turnover characteristic of Ras-transformation may maintain YAP in a hyper-active form (Figure 5f). One scenario is that the enhanced chromatin interaction of YAP in MCF10A cells constitutes a nonspecific retention mechanism geared towards YAP deactivation. Tyrosine phosphorylation of nuclear YAP at Y357 has been shown to reduce its transcriptional competence without affecting its localization. It will be an important next step to address whether spatial resets can reverse a nucleus specific inhibitory modification (*19*).

Materials and Methods

Cell culture

MCF10A, MCF10AT were cultured as previously described (*60*). SUM159, MDA-MB-231 were cultured in DMEM + 10% FBS. All cell lines were maintained at 37° C and 5% CO_2 either in tissue culture incubators or microscope incubators.

Drug treatments

Thapsigargin (TG): Alfa Aesar - #J62866. 1mM DMSO stock. Cells were treated at 1 μM and imaged immediately.
Src inhibitor (PP1): Cayman Chemical Company - #14244. 10mM DMSO stock. Cells were treated at 10 μM and imaged after 1 hr for YAP fluctuation experiments or immediately for transcription experiments.
PKC inhibitor (Go 6976): Tocris, #2253. 1mM DMSO stock. Cells were treated at 1 μM for 2 hours before being treated by TG.

Cell line generation and endogenous gene tagging using CRISPR-Cas9

For C terminal tagging of YAP and TEAD with GFP/mCherry we generated donor plasmids for homology dependent repair (HDR) where the general design of the donor plasmid consisted of an upstream homology arm (~1Kb long) followed by GFP/mCherry-(P2A-Puromycin/Hygromycin-stop codon) cassette followed by a downstream homology arm (~1Kb long). MCF10A cells grown to ~80% confluence were trypsinized and electroporated with the donor plasmid, guide RNA plasmid and a plasmid expressing SpCas9 at a ratio of 2:1:1 (total 12ug) using Neon electroporator (Life Technologies) and a 30ms: 1100V: 2pulse electroporation program. Following electroporation cells were grown for three days before initiating antibiotic selection. For antibiotic selection, fresh media containing 1μg/ml Puromycin or 250 μg/ml Hygromycin was added to the cells every two days. Post selection cells were grown in antibiotic free media. For both YAP and TEAD, tagging efficiency was nearly 100% as nearly all cells post-selection showed appropriate localization of the FP tagged proteins and were genomically stable over at least 20 division cycles. For further validation genomic sequences containing the knockins were PCR amplified and sequenced. For generating YAP GFP knockins of MCF10AT, SUM159 and MDA-MB231, cells were electroporated using a Neon electroporator then selected as described above. For MDA-MB231 a 10ms: 1400V: 4pulse electroporation program was used whereas for MCF10AT and SUM159 we used a 30ms: 1100V: 2pulse electroporation program.

For generating cell lines that can report on native transcription kinetics of YAP responsive genes, MCF10A cells were first transfected with a Super Piggy BAC Transposase expression vector (SBI) and a custom generated PiggyBAC vector carrying an MCP-mNeon gene driven by TRE3G promoter and a rTTA3 (tetracycline-controlled transactivator 3)-T2A-Hygromycin cassette driven by a PGK promter, followed by selection with 250ug/ml hygromycin. To insert a 24X MS2 transcription reporter cassette at the beginning of the 3' UTR of AREG, we generated a donor plasmid for homology dependent knockin where the general design consisted of an upstream homology arm (~1Kb long) followed by a HA tag-P2A-Blasticidine-stop codon-24X MS2 cDNA cassette followed by a downstream homology arm (~1Kb long). For ANKRD1, which had a low CRISPR mediated knockin efficiency, we used a double cut HDR donor plasmid where the "homology-knockin" cassette was flanked by single guide RNA (sgRNA)-PAM sequence on either side. This greatly increased knockin efficiency for ANKRD1. Cells were selected with 10 μg/ml Blastcidine.

For calcium sensing, cells were transduced with lentiviral particles reconstituted from a lentiviral vector expressing GcAMP6f from a constitutively active CMV promoter.

To minimize any potential confounding effect of differences in source of origin of MCF10A and MCF10AT, we generated a constitutively active H-Ras (H-RasG12V) transformed MCF10AYAP-GFP-KI cell line using lentiviral transduction and subsequent selection for neomycin resistance using Geneticin (400 µg/mL). This cell line was used specifically for the line-FRAP, and import/export measurements.

Details of Cell lines

Cell line	Source cell line	Method of cell line generation	Antibiotic resistance
MCF 10A YAP-eGFP	MCF10A	CRISPR knock in	Puromycin
MCF 10AT YAP-eGFP	MCF10AT	CRISPR knock in	Puromycin
MCF 10AT YAP-eGFP	MCF10A YAP-eGFP	CRISPR knock in + HRas Lentiviral transduction	Neomycin
SUM159 YAP-eGFP	SUM159	CRISPR knock in	Puromycin
MDA MB 231 YAP-eGFP	MDA MB 231	CRISPR knock in	Puromycin
MCF 10A YAP-eGFP + TEAD1 mCherry	MCF10A	Dual CRISPR knock in	Puromycin + Hygromycin
MCF 10A TEAD1 eGFP	MCF10A	CRISPR knock in	Hygromycin
MCF 10A MCP mNeon	MCF10A	PiggyBAC transposition	Hygromycin
MCF 10A MCP mNeon Areg 24X MS2	MCF10A MCP mNeon	CRISPR knock in	Hygromycin + Blasticidin
MCF 10A MCP mNeon ANKRD1 24X MS2	MCF10A MCP mNeon	CRISPR knock in	Hygromycin + Blasticidin
MCF 10A GcAMP6f	MCF 10A	Lenti Viral transduction	Puromycin
MCF10A YAP-eGFP + LAM del50 mCherry	MCF 10A YAP-eGFP	PiggyBAC transposition	Hygromycin
MCF 10A NLS-GFP_{2X}-NES	MCF 10A	Lenti Viral transduction	Neomycin
MCF 10AT NLS-GFP_{2X}-NES	MCF 10AT	Lenti Viral transduction	Neomycin
SUM 159 NLS-GFP_{2X}-NES	SUM 159	Lenti Viral transduction	Neomycin
MDA MB231 NLS-GFP_{2X}-NES	MDA MB231	Lenti Viral transduction	Neomycin

Guide sequences used for CRISPR knockin

YAP	TTAGAATTCAGTCTGCCTGA
TEAD	GGCTTGTAAAGGACTGAACA
AREG	AAGAAACTTCGACAAGAGAA
ANKRD1	TCTCGCATAGCTACATTCTG

Microscopy

Live imaging was done on either Zeiss LSM700 or an Olympus FV10i. Cells plated on fibronectin-coated Mattek dishes (35mm, No. 1.5 glass) were imaged either with 63x/1.40 oil immersion (Zeiss) or 60x/1.2 water immersion (Olympus) objective. All multi-day image acquisitions were carried out on Olympus FV10i.

All photo-bleaching experiments were performed on Zeiss LSM700 using the following setup.

Photobleaching experiments	Laser (nm)	Frame rate	# pre-scan frames	# bleach scans	# post-scan frames
Import/export	488	10 s	1	12	12
YAP spatiotemporal FRAP	488	4.6 ms	500	8	1000

Image analysis

All calculations and analysis were performed using MATLAB, Python, and ImageJ. The functions are publicly available here: https://github.com/jmfrank/track_analyzer. FRAP model fitting was implemented in Mathematica based on Stasevich et al (*57*).

Cell tracking

Cell tracking was performed following these steps: (1) anisotropic diffusion filtering and sum of signal derivatives (*61*), (2) applying global threshold to identify nuclei, (3) seeded watershed segmentation to breakup regions into single nuclei, (4) frame-to-frame tracking using a distance minimizing linking algorithm. Tracking was verified by eye using a GUI, and artefactual tracks were flagged and excluded by downstream analysis.

N/C ratio

In this work, the N/C ratio is defined as the ratio of nuclear to cytoplasmic concentrations of YAP (or TEAD), assessed by the mean fluorescence intensity in the nucleus and cytoplasmic volumes after subtracting fluorescence background. Using the nucleus boundary generated by Sir-DNA image segmentation, the plane with maximal intensity. Because YAP is physically excluded from the nucleoli, we removed the nucleolar regions (determined by the lower 35th percentile of intensities within the nucleus boundary). The cytoplasmic region was determined by generating a mask extending 0.5 um from the nucleus boundary into the cytoplasm. Because TEAD is mostly nuclear, we used the TEAD signal to segment the nucleus and assessed N/C as done with YAP.

Local cell density

To account for variable density in a growing monolayer, we estimated the local cell density for each detected cell as the number of cell centroids found within a search radius of 250 pixels (69 μm) of the cell of interest centroid.

YAP N/C fluctuation analysis

Rapid changes in YAP signal were defined as signals that are continuously increasing or decreasing by at least 0.12. If the signal did not change at least 0.005 over a 3-frame window, then the signal was considered stagnated and continuity was broken.

Wound assay

MCF10A cells were seeded on MATTEK imaging dishes at 50% confluency. After 3 days of growth, the very dense monolayer was imaged (Figure 3a pre-wound). The dish was then gently scratched with a 20uL pipette tip and immediately imaged. About a 1-minute delay between wounding and the first image due to incubator adjustment and microscope focusing.

GcAMP6f imaging

Similar to the YAP signal, we measured the GcAMP6f signal as the average of a 0.5 um wide contour extending into the cytoplasm from the nuclear boundary, as the GcAMP6f signal is relatively depleted inside the nucleus.

Nascent transcription

Nucleus segmentation was performed in 3D to ensure each nascent transcription spot was located within the nucleus. Although we sorted MCP-mNeon expressing cells, the expression per cell was variable, requiring a local thresholding technique to segment cells with different expression levels. This was done using the following steps:
[1] Applying filtering (as described in the 2D Sir-DNA segmentation)
[2] Finding local maxima in the field
[3] Applying a lower-bound threshold to segment all regions containing a local maxima
[4] Looping over all regions found in 3 and using the derivative of the intensity-percentile distribution (dI/dP) of pixel intensities to determine the local threshold. A peak in dI/dP indicates the background to foreground boundary (see plot below). With no significant peak, the region is properly segmented. Because the local threshold is not the same for all regions, one needs to look at the histogram information in terms of percentile to find the foreground vs background for each sub-region.

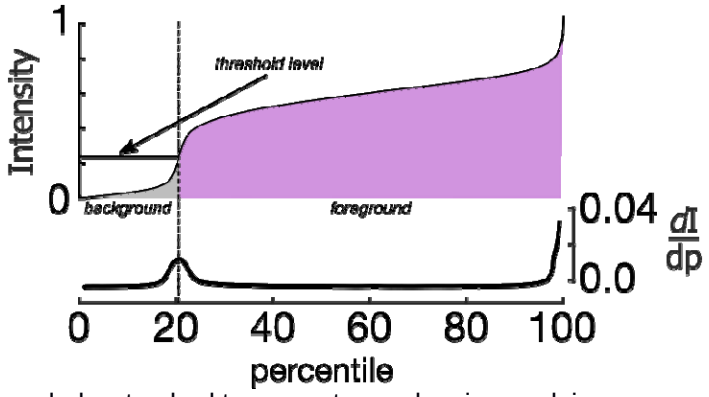

[5] Applying a seeded watershed to separate overlapping nuclei.

After identifying cell nuclei, actively transcribing cells were identified by looking for a sharp, bright signal (for MCP-mNeon) within the segmented nuclei. Spots were detected in two steps to ensure robust quantification:

[1] Potential spots were first identified by using a Laplacian of Gaussian filter, followed by a local thresholding by identifying potential spots as regions of pixel intensity greater than 99.97th percentile of all pixels within a particular nucleus.

[2] An integrated intensity threshold is then applied to these potential spots from step 1. For each potential spot, a background measurement was made using a shell mask centered at the centroid of the potential spot (inner diameter 7px, outer diameter 9 pixels). The integrated intensity is the sum of all pixel values within the inner shell region (i.e. pixels located less than 3.5 pixels from centroid).

[3] Particle tracking was applied to nascent spots to gather statistics on pulse duration and intensity.

Analysis of mitotic cells

Cells going through mitosis were manually annotated using a GUI to mark the time of cytokinesis, parent cell, and daughter cells for each division. The data extracted from the cells is then aligned by the time of cytokinesis. To create the YAP N/C trace through division, the N/C trace of the parent cell was concatenated with the mean N/C values of the daughter cells. Nascent transcription through mitosis was evaluated by measuring the fraction of cells with at least one nascent transcription spot, and normalizing the pre-mitosis fraction to 1. Because the pre-mitosis nucleus is diploid, there are 2X copies of the MS2 gene cassette and each daughter receives 1X copies. Therefore, the post-mitosis fraction of cells is measured by whether *either* of the daughters are transcribing, which means the same number of MS2 gene cassettes are monitored before and after division.

Spatiotemporal line FRAP of nuclear YAP-eGFP

We found that the YAP-eGFP recovery is extremely rapid, so we opted to use a circular ROI for bleaching (10 pixel radius, 0.9 μm) but a line ROI (2 pixel wide) bisecting the bleach spot to monitor the recovery, allowing a 4.6 millisecond frame time using the Ziess 700. For each bleach acquisition, a background measurement was taken at the same position after waiting 15 seconds after the bleach acquisition completed. The final spatiotemporal recovery curve was generated by: (1) Normalizing fluorescence and correcting for acquisition bleaching, (2) averaging across the 2-pixel wide line, and (3) finding the bleach-center by Gaussian fitting and then averaging across the bleach center. First, we fit the mean recovery curve for each condition to both a pure diffusion and reaction-diffusion model (Supplementary Figure 6). In order to estimate the experimental error for the parameters, we fit 30 bootstrapped samplings (5 experiments per bootstrap) as individual experiments were too noisy to provide accurate fits to the models. The data in Supplementary Table 1 is the mean and standard deviation of each parameter from the 30 bootstraps samples.

For MCF10A, the reaction-diffusion model fit decreased sum of squared residuals (SSD), while the pure diffusion model provided an unrealistically low diffusion rate, suggesting that significant binding accounts the relatively slow FRAP recovery. For MCF10A+HRas, SUM159, and MDA-MB-231, the reaction-diffusion model slightly decreased SSD compared to pure-diffusion, however the effective diffusion was very large, ranging between 38 and 45 $\mu m^2/s$, while the pure diffusion model diffusion coefficient ranged between 24 and 26 $\mu m^2/s$. Previously reported work suggests that the diffusion coefficient for a 100 kDa protein is approximately 21 $\mu m^2/s$ (*62*). Therefore, believe that YAP kinetics in

MCF10A+HRas, SUM159, and MDA-MB-231 are best described by pure-diffusion, and binding is negligible at the experimental resolution we could achieve.

Import / export rates of YAP and synthetic NLS-NES construct

The first-order nuclear import and export rate of either YAP or the NLS-NES construct (NLS-GFP2X-NES) was measured by monitoring the nuclear intensity after bleaching either the nucleus or cytoplasm. First, a bright field image was used to draw a spline ROI defining the contour of the nucleus or cytoplasm. After bleaching ROI, time-lapse confocal imaging was used to monitor the recovery. We found that full recovery of YAP after nuclear/cytoplasm bleaching was on the time-scale of ~1-2 minutes. As nuclear volume is essentially constant on this time scale, and YAP signal is homogenous and rapidly diffuses, we measured the average fluorescence intensity of an ROI within the nucleus over time. We then monitored the change of this signal from the first post-bleach time point. The first-order import or export rate is then approximated by the slope of a linear fit to the change in signal intensity over the first 30 seconds (frames 1-4) after bleaching.

RNA-seq relative gene expression

Raw reads of RNA-seq for MCF10A and MCF10AT were downloaded from GEO-Depositions (MCF10A-HRas: GSE81593(*63*); MCF10A: GSE75168 (*64*)). The reads were first trimmed with cutadapt to remove adapters and low quality reads. The reads then were aligning to human genome hg19 using HISAT2 with default parameters. Gene expression counts were obtained from bam files using htseq-count.

Acknowledgments

This work was partially supported by the National Institutes of Health (NIH) National Institute Of General Medical Sciences (NIGMS)/National Cancer Institute (NCI) Grant GM77856, NCI Physical Sciences Oncology Center Grant U54CA143836, National Science Foundation Graduate Fellowship Program #DGE-114747, and National Institute Of Biomedical Imaging And Bioengineering (NIBIB)/4D Nucleome Roadmap Initiative 1U01EB021237.

Author Contributions

R.P.G and J.M.F and J.T.L conceived the project. J.M.F and R.P.G designed research. R.P.G did most of the genome editing using CRISPR/Cas9. J.M.F, R.P.G and Q.S did experiments. J.M.F analyzed most of the data. R.P.G, J.M.F and J.T.L wrote the paper.

References

1. D. Mullassery, C. A. Horton, C. D. Wood, M. R. H. White, Single live-cell imaging for systems biology 9. *Essays Biochem.* (2008), doi:10.1042/bse0450121.
2. S. D. M. Santos, P. J. Verveer, P. I. H. Bastiaens, Growth factor-induced MAPK network topology shapes Erk response determining PC-12 cell fate. *Nat. Cell Biol.* (2007), doi:10.1038/ncb1543.
3. J. E. Purvis, G. Lahav, Encoding and decoding cellular information through signaling dynamics. *Cell* (2013), , doi:10.1016/j.cell.2013.02.005.
4. E. Batchelor, A. Loewer, C. Mock, G. Lahav, Stimulus-dependent dynamics of p53 in single cells. *Mol. Syst. Biol.* (2011), doi:10.1038/msb.2011.20.
5. L. Ashall *et al.*, Pulsatile stimulation determines timing and specificity of NF-κB-dependent transcription. *Science (80-.).* (2009), doi:10.1126/science.1164860.
6. S. M, Yes-associated protein (YAP65) is a proline-rich phosphoprotein that binds to the SH3 domain of the Yes proto-oncogene product.le. *Oncogene* (1994).
7. F. Kanai *et al.*, TAZ: A novel transcriptional co-activator regulated by interactions with 14-3-3 and PDZ domain proteins. *EMBO J.* (2000), doi:10.1093/emboj/19.24.6778.
8. T. Moroishi, C. G. Hansen, K. L. Guan, The emerging roles of YAP and TAZ in cancer. *Nat. Rev. Cancer* (2015), doi:10.1038/nrc3876.
9. F. Zanconato, M. Cordenonsi, S. Piccolo, YAP/TAZ at the Roots of Cancer. *Cancer Cell* (2016), , doi:10.1016/j.ccell.2016.05.005.
10. S. Dupont *et al.*, Role of YAP/TAZ in mechanotransduction. *Nature* (2011), doi:10.1038/nature10137.
11. G. Halder, S. Dupont, S. Piccolo, Transduction of mechanical and cytoskeletal cues by YAP and TAZ. *Nat. Rev. Mol. Cell Biol.* (2012), , doi:10.1038/nrm3416.
12. M. Aragona *et al.*, A mechanical checkpoint controls multicellular growth through YAP/TAZ regulation by actin-processing factors. *Cell* (2013), doi:10.1016/j.cell.2013.07.042.
13. B. Zhao *et al.*, Inactivation of YAP oncoprotein by the Hippo pathway is involved in cell contact inhibition and tissue growth control. *Genes Dev.* (2007), doi:10.1101/gad.1602907.
14. B. Zhao *et al.*, TEAD mediates YAP-dependent gene induction and growth control. *Genes Dev.* (2008), doi:10.1101/gad.1664408.
15. F. Zanconato *et al.*, Genome-wide association between YAP/TAZ/TEAD and AP-1 at enhancers drives oncogenic growth. *Nat. Cell Biol.* (2015), doi:10.1038/ncb3216.
16. C. Stein *et al.*, YAP1 Exerts Its Transcriptional Control via TEAD-Mediated Activation of Enhancers. *PLoS Genet.* (2015), doi:10.1371/journal.pgen.1005465.
17. D. Elster *et al.*, TRPS1 shapes YAP/TEAD-dependent transcription in breast cancer cells. *Nat. Commun.* (2018), doi:10.1038/s41467-018-05370-7.
18. A. Elosegui-Artola *et al.*, Force Triggers YAP Nuclear Entry by Regulating Transport across Nuclear Pores. *Cell* (2017), doi:10.1016/j.cell.2017.10.008.
19. N. Ege *et al.*, Quantitative Analysis Reveals that Actin and Src-Family Kinases Regulate Nuclear YAP1 and Its Export. *Cell Syst.* (2018), doi:10.1016/j.cels.2018.05.006.
20. S. A. Manning *et al.*, Dynamic Fluctuations in Subcellular Localization of the Hippo Pathway Effector Yorkie In Vivo. *Curr. Biol.* (2018), doi:10.1016/j.cub.2018.04.018.
21. J. Wang, J. Sinnett-Smith, J. V. Stevens, S. H. Young, E. Rozengurt, Biphasic regulation of Yes-associated Protein (YAP) cellular localization, phosphorylation, and activity by G proteincoupled receptor agonists in intestinal epithelial cells: A novel role for Protein Kinase D (PKD). *J. Biol. Chem.* **291**, 17988–18005 (2016).
22. L. Cong *et al.*, Multiplex genome engineering using CRISPR/Cas systems. *Science (80-.).* (2013), doi:10.1126/science.1231143.
23. P. Mali *et al.*, RNA-guided human genome engineering via Cas9. *Science (80-.).* (2013), doi:10.1126/science.1232033.
24. A. Raj, C. S. Peskin, D. Tranchina, D. Y. Vargas, S. Tyagi, Stochastic mRNA synthesis in mammalian cells. *PLoS Biol.* (2006), doi:10.1371/journal.pbio.0040309.
25. D. M. Suter *et al.*, Mammalian genes are transcribed with widely different bursting kinetics. *Science (80-.).* (2011), doi:10.1126/science.1198817.
26. D. M. Suter, N. Molina, F. Naef, U. Schibler, Origins and consequences of transcriptional discontinuity. *Curr. Opin. Cell Biol.* (2011), , doi:10.1016/j.ceb.2011.09.004.

27. K.-C. Wang *et al.*, Flow-dependent YAP/TAZ activities regulate endothelial phenotypes and atherosclerosis. *Proc. Natl. Acad. Sci.* (2016), doi:10.1073/pnas.1613121113.
28. J. Zhang *et al.*, YAP-dependent induction of amphiregulin identifies a non-cell-autonomous component of the Hippo pathway. *Nat. Cell Biol.* (2009), doi:10.1038/ncb1993.
29. J. Russo, L. Tait, I. H. Russo, Morphological expression of cell transformation induced by c-Ha-ras oncogene in human breast epithelial cells. *J Cell Sci* (1991).
30. B. V. V. G. Reddy, K. D. Irvine, Regulation of Hippo Signaling by EGFR-MAPK Signaling through Ajuba Family Proteins. *Dev. Cell* (2013), doi:10.1016/j.devcel.2013.01.020.
31. S. J. Rawat *et al.*, H-ras Inhibits the Hippo Pathway by Promoting Mst1/Mst2 Heterodimerization. *Curr. Biol.* (2016), doi:10.1016/j.cub.2016.04.027.
32. K. C. Lin *et al.*, Regulation of Hippo pathway transcription factor TEAD by p38 MAPK-induced cytoplasmic translocation (Nature Cell Biology, (2017), 19, 8, (996-1002), 10.1038/ncb3581). *Nat. Cell Biol.* **20**, 1098 (2018).
33. Z. Meng, T. Moroishi, K. L. Guan, Mechanisms of Hippo pathway regulation. *Genes Dev.* (2016), , doi:10.1101/gad.274027.115.
34. N. G. Kim, B. M. Gumbiner, Adhesion to fibronectin regulates Hippo signaling via the FAK-Src-PI3K pathway. *J. Cell Biol.* (2015), doi:10.1083/jcb.201501025.
35. Y. Si *et al.*, Src Inhibits the hippo tumor suppressor pathway through tyrosine phosphorylation of Lats1. *Cancer Res.* (2017), doi:10.1158/0008-5472.CAN-17-0391.
36. J. H. Hanke *et al.*, Discovery of a novel, potent, and Src family-selective tyrosine kinase inhibitor: Study of Lck- and FynT-dependent T cell activation. *J. Biol. Chem.* (1996), doi:10.1074/jbc.271.2.695.
37. K. Sato, Y. Ito, T. Yomo, K. Kaneko, On the relation between fluctuation and response in biological systems. *Proc. Natl. Acad. Sci.* (2003), doi:10.1073/pnas.2334996100.
38. P. J. Sammak, L. E. Hinman, P. O. Tran, M. D. Sjaastad, T. E. Machen, How do injured cells communicate with the surviving cell monolayer? *J. Cell Sci.* (1997).
39. V. E. Klepeis, A. Cornell-Bell, V. Trinkaus-Randall, Growth factors but not gap junctions play a role in injury-induced Ca2+ waves in epithelial cells. *J Cell Sci* (2001), doi:10.1016/j.jana.2012.06.007.
40. P. Niethammer, C. Grabher, A. T. Look, T. J. Mitchison, A tissue-scale gradient of hydrogen peroxide mediates rapid wound detection in zebrafish. *Nature* (2009), doi:10.1038/nature08119.
41. C. Justet, J. A. Hernández, A. Torriglia, S. Chifflet, Fast calcium wave inhibits excessive apoptosis during epithelial wound healing. *Cell Tissue Res.* (2016), doi:10.1007/s00441-016-2388-8.
42. J. Lytton, M. Westlin, M. R. Hanley, Thapsigargin inhibits the sarcoplasmic or endoplasmic reticulum Ca-ATPase family of calcium pumps. *J. Biol. Chem.* (1991), doi:VL - 266.
43. T. W. Chen *et al.*, Ultrasensitive fluorescent proteins for imaging neuronal activity. *Nature* (2013), doi:10.1038/nature12354.
44. J. Lembong, B. Sabass, H. A. Stone, Calcium oscillations in wounded fibroblast monolayers are spatially regulated through substrate mechanics. *Phys. Biol.* (2017), doi:10.1088/1478-3975/aa6b67.
45. A. J. Morgan, R. Jacob, Ionomycin enhances Ca^{2+} influx by stimulating store-regulated cation entry and not by a direct action at the plasma membrane. *Biochem. J.* (1994), doi:10.1042/bj3000665.
46. P. Wang *et al.*, PP1A-mediated dephosphorylation positively regulates YAP2 activity. *PLoS One* (2011), doi:10.1371/journal.pone.0024288.
47. E. M. Schwiebert, A. Zsembery, Extracellular ATP as a signaling molecule for epithelial cells. *Biochim. Biophys. Acta - Biomembr.* (2003), , doi:10.1016/S0005-2736(03)00210-4.
48. K. Nishi *et al.*, Leptomycin B targets a regulatory cascade of crm1, a fission yeast nuclear protein, involved in control of higher order chromosome structure and gene expression. *J. Biol. Chem.* (1994), doi:10.1002/nur.10107.
49. Z. Liu *et al.*, Induction of store-operated calcium entry (SOCE) suppresses glioblastoma growth by inhibiting the Hippo pathway transcriptional coactivators YAP/TAZ. *Oncogene* (2018), , doi:10.1038/s41388-018-0425-7.
50. J. Swift *et al.*, Nuclear lamin-A scales with tissue stiffness and enhances matrix-directed differentiation. *Science (80-.).* (2013), doi:10.1126/science.1240104.
51. S. Cho, J. Irianto, D. E. Discher, Mechanosensing by the nucleus: From pathways to scaling relationships. *J. Cell Biol.* (2017), , doi:10.1083/jcb.201610042.

52. S. Osmanagic-Myers, T. Dechat, R. Foisner, Lamins at the crossroads of mechanosignaling. *Genes Dev.* (2015), , doi:10.1101/gad.255968.114.
53. Y. Liu *et al.*, YAP modulates TGF-β1-induced simultaneous apoptosis and EMT through upregulation of the EGF receptor. *Sci. Rep.* (2017), doi:10.1038/srep45523.
54. W. Akhtar *et al.*, Chromatin position effects assayed by thousands of reporters integrated in parallel. *Cell* (2013), doi:10.1016/j.cell.2013.07.018.
55. E. Bertrand *et al.*, Localization of ASH1 mRNA particles in living yeast. *Mol. Cell* (1998), doi:10.1016/S1097-2765(00)80143-4.
56. N. C. Shaner *et al.*, A bright monomeric green fluorescent protein derived from Branchiostoma lanceolatum. *Nat. Methods* (2013), doi:10.1038/nmeth.2413.
57. T. J. Stasevich, F. Mueller, D. T. Brown, J. G. McNally, Dissecting the binding mechanism of the linker histone in live cells: An integrated FRAP analysis. *EMBO J.* (2010), doi:10.1038/emboj.2010.24.
58. M. Xue *et al.*, Frequency modulated translocational oscillations of Nrf2, a transcription factor functioning like a wireless sensor. *Biochem. Soc. Trans.* (2015), doi:10.1042/BST20150060.
59. M. Xue *et al.*, Frequency Modulated Translocational Oscillations of Nrf2 Mediate the Antioxidant Response Element Cytoprotective Transcriptional Response. *Antioxid. Redox Signal.* (2015), doi:10.1089/ars.2014.5962.
60. J. Debnath, S. K. Muthuswamy, J. S. Brugge, Morphogenesis and oncogenesis of MCF-10A mammary epithelial acini grown in three-dimensional basement membrane cultures. *Methods* (2003), , doi:10.1016/S1046-2023(03)00032-X.
61. B. Rajasekaran, K. Uriu, G. Valentin, J. Y. Tinevez, A. C. Oates, Object segmentation and ground truth in 3D embryonic imaging. *PLoS One* (2016), doi:10.1371/journal.pone.0150853.
62. N. Dross *et al.*, Mapping eGFP oligomer mobility in living cell nuclei. *PLoS One* (2009), doi:10.1371/journal.pone.0005041.
63. K. E. Yoh *et al.*, Repression of p63 and induction of EMT by mutant Ras in mammary epithelial cells. *Proc. Natl. Acad. Sci.* (2016), doi:10.1073/pnas.1613417113.
64. T. L. Messier *et al.*, Histone H3 lysine 4 acetylation and methylation dynamics define breast cancer subtypes. *Oncotarget* (2016), doi:10.18632/oncotarget.6922.

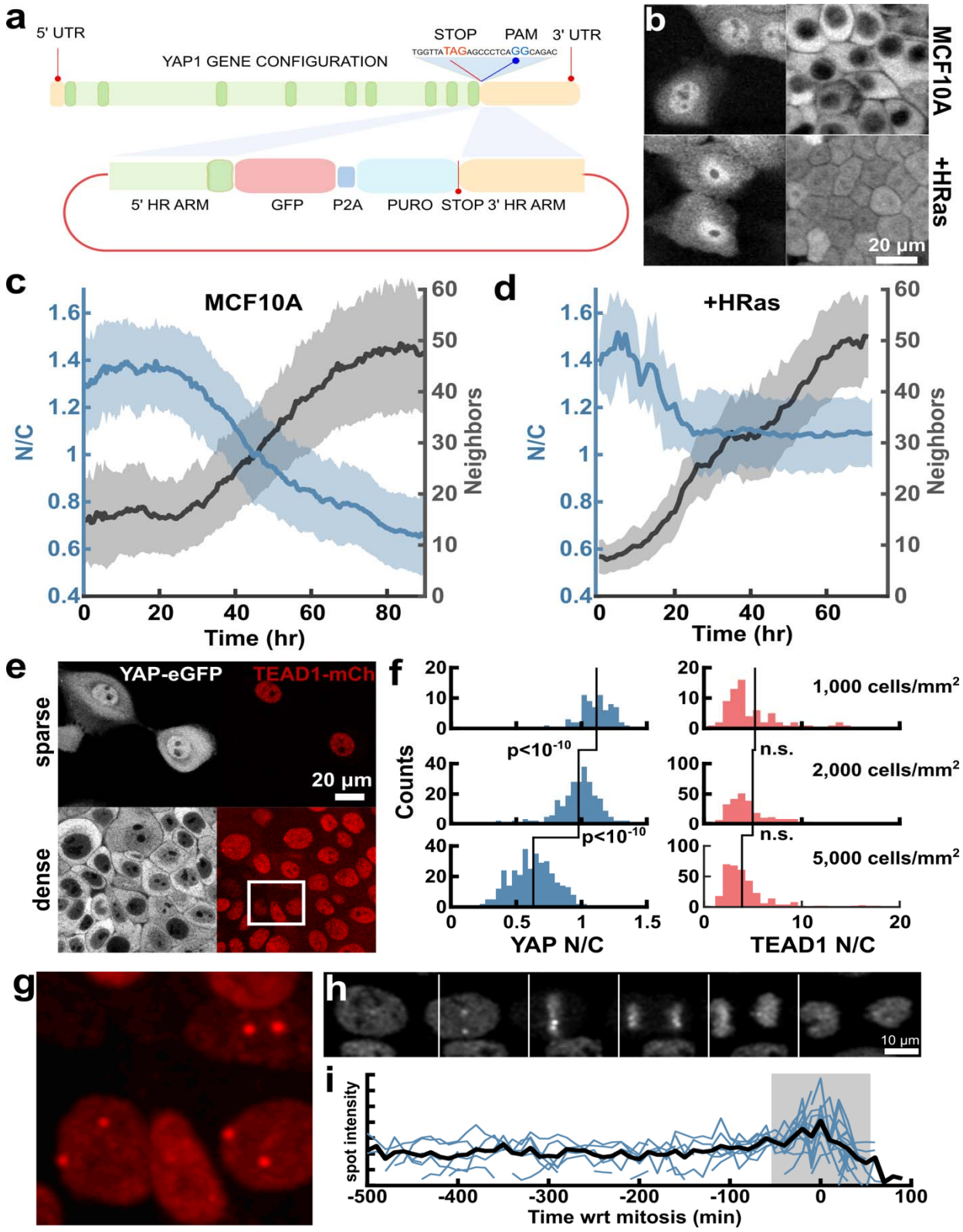
a
5' UTR
YAP1 GENE CONFIGURATION
STOP
PAM
3' UTR
TGGTTATAGAGCCCTCAGGCAGAC
5' HR ARM
GFP
P2A
PURO
STOP
3' HR ARM
b
MCF10A
+HRas
20 µm
c
MCF10A
N/C
Neighbors
Time (hr)
d
+HRas
N/C
Neighbors
Time (hr)
e
YAP-eGFP
TEAD1-mCh
sparse
dense
20 µm
f
Counts
p<10^-10
p<10^-10
n.s.
n.s.
1,000 cells/mm²
2,000 cells/mm²
5,000 cells/mm²
YAP N/C
TEAD1 N/C
g
h
10 µm
i
spot intensity
Time wrt mitosis (min)

Figure 1: **Characterization of YAP and TEAD genome-knockin cell lines**. (**a**) Cartoon of CRISPR-Cas9 based insertion of eGFP-P2A-puromycin cassette at 3' end of the YAP gene. (**b**) Native YAP-eGFP expression/localization in sparse and dense cultures of MCF10A and MCF10A-HRas (MCF10AT). (**c, d**) Time-lapse of YAP-eGFP nuclear/cytoplasmic ratio (N/C) during monolayer growth for MCF10A (N=915 cell tracks) (c), MCF10AT (N=1478 cell tracks) (d). (**e**) Dense and sparse MCF10A cells with YAP-eGFP and TEAD1-mCherry dual CRISPR knockin. (**f**) N/C of YAP and TEAD1 in MCF10A as a function of density. (**g**) TEAD1-mCherry in MCF10A shows focal accumulation to a potentially genomically defined region. (**h**) A dividing MCF10A cell showing TEAD1-eGFP spot arrangement at different stages of division. (**i**) Time course of TEAD1 spot intensity through cell division (data from 5 dividing cells). Gray shaded region denotes mitosis.

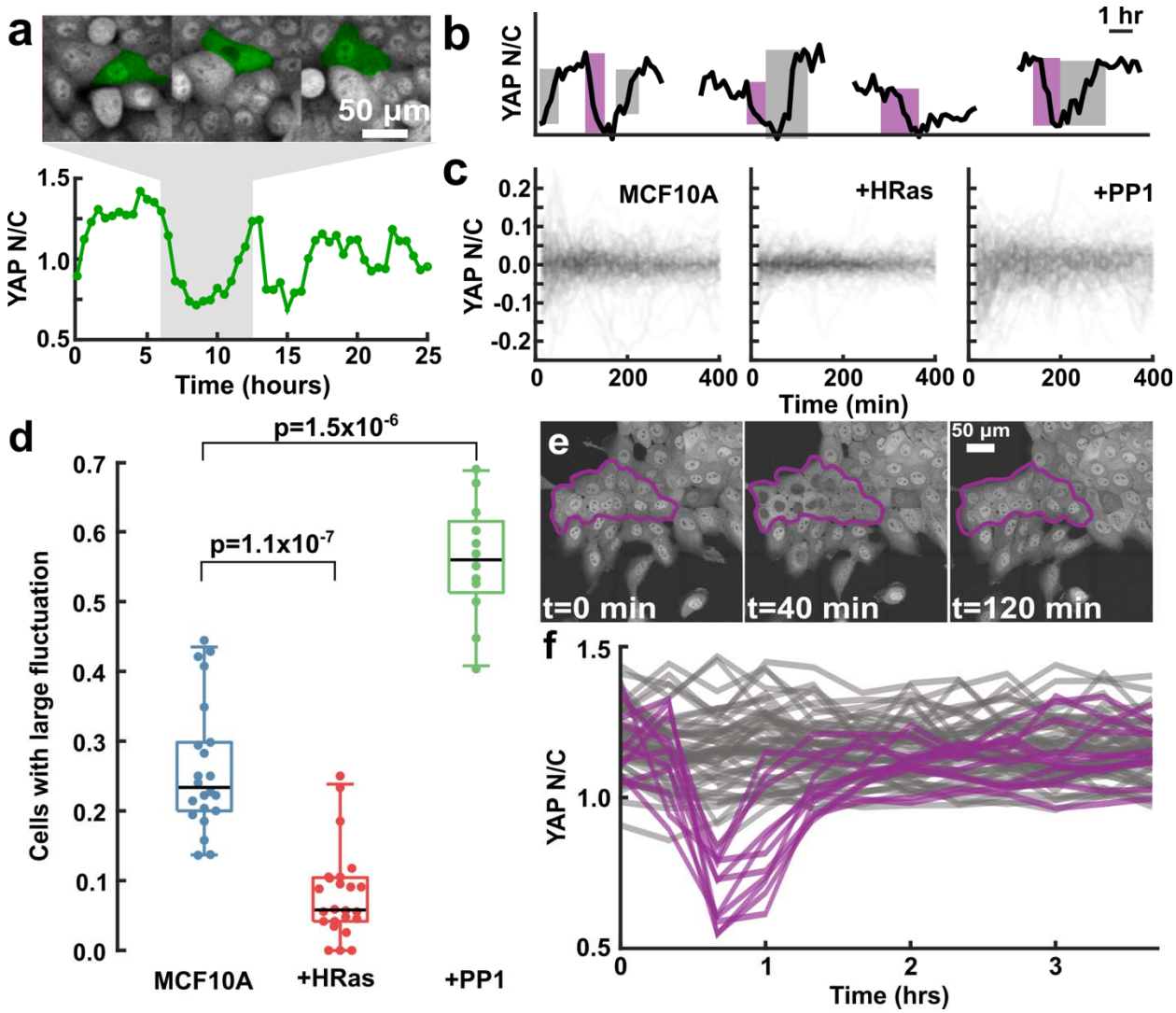

Figure 2: Baseline (minute-scale) fluctuations in YAP localization. (**a**) N/C trace of an individual MCF10A cell in monolayer and corresponding fluorescence image (cell of interest is false-colored in green). (**b**) Example traces of YAP N/C over time with large changes in signal highlighted by grey (increase) and purple (decrease) in MCF10A cells. (**c**) Overlay of YAP N/C traces for MCF10A, MCF10A+HRas, and MCF10A+PP1. Each plot contains 200 traces randomly selected from the pool of all tracks collected from each condition. The mean value is subtracted from each trace to allow visual comparison. (**d**) Mean fraction of cells per ROI (0.0171 mm^2) with at least one detectable fluctuation (24 ROIs for each condition compiled from two independent experiments). (**e-f**) Local cluster of cells showing a coordinated spatial-reset of YAP. (**e**) Fluorescence images of cells at different stages of coordinated spatial reset. (**f**) YAP N/C traces for cells showing coordinated fluctuation (purple) and cells showing invariant YAP N/C (gray).

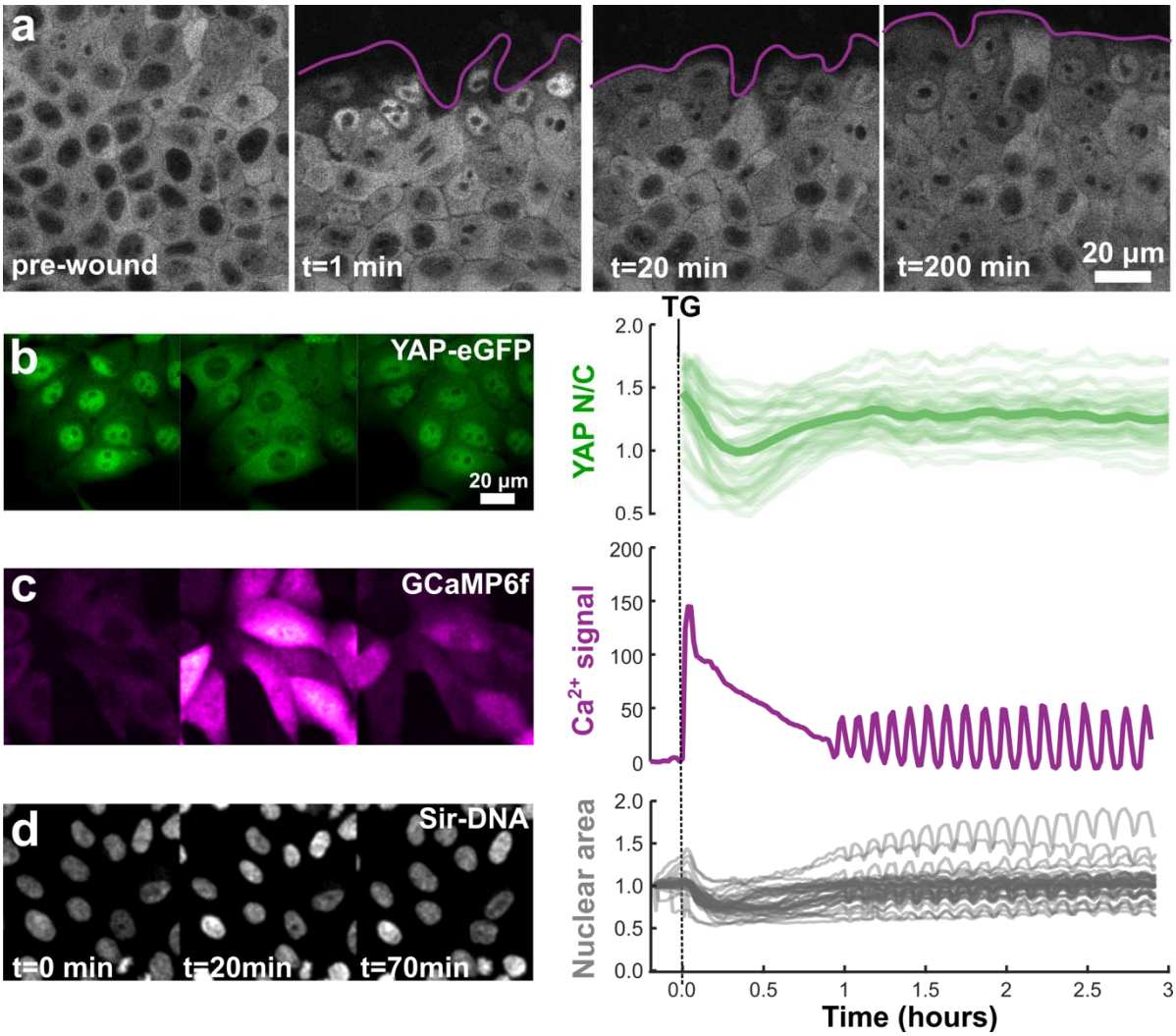

Figure 3: Calcium signaling induces YAP spatial-reset and concomitant changes in nuclear morphology. (**a**) Time course of YAP-eGFP localization in MCF10A cells at a wound edge. Wound edge highlighted in magenta. (**b-d**) YAP localization (**b**), cytoplasmic calcium signal (**c**) and, nuclear shape (**d**) at different time points after induction of SOCE using 1uM thapsigargin. YAP N/C traces are from 43 cells and 2 independent experiments. Nuclear area trace and GCaMP6f Ca^{2+} trace are from 42 cells and 2 independent experiments.

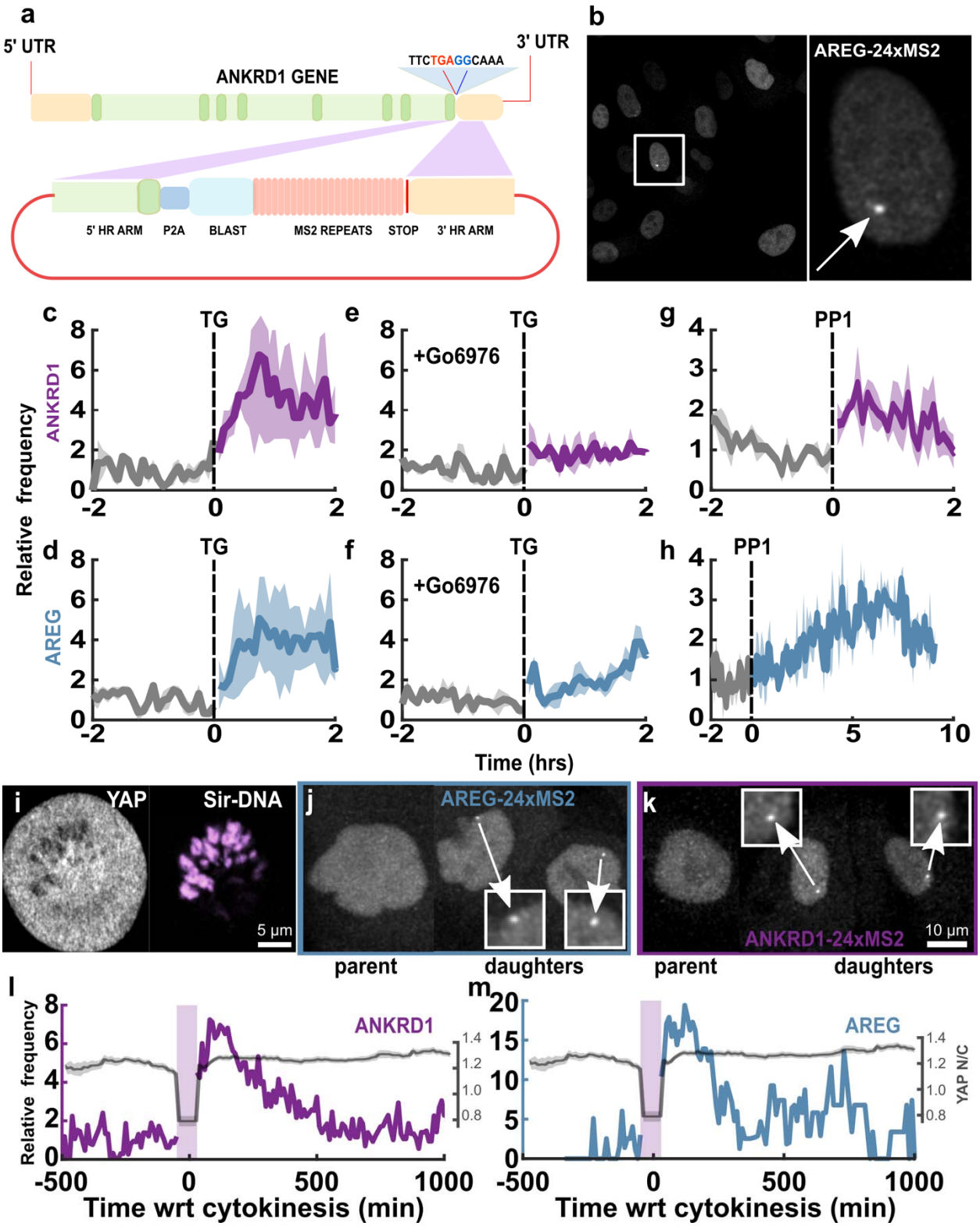
a
5' UTR
3' UTR
ANKRD1 GENE
TTCTGAGGCAAA
5' HR ARM
P2A
BLAST
MS2 REPEATS
STOP
3' HR ARM
b
AREG-24xMS2
c
TG
ANKRD1
e
TG
+Go6976
g
PP1
d
TG
AREG
f
TG
+Go6976
h
PP1
Relative frequency
Time (hrs)
i
YAP
Sir-DNA
5 µm
j
AREG-24xMS2
parent
daughters
k
ANKRD1-24xMS2
10 µm
parent
daughters
l
ANKRD1
Relative frequency
YAP N/C
Time wrt cytokinesis (min)
m
AREG
YAP N/C
Time wrt cytokinesis (min)

Figure 4: Transcription dynamics of YAP target genes. (**a**) Cartoon showing strategy for knocking in an MS2 transcription reporter cassette at the end of the coding sequence of ANKRD1 gene. (**b**) Representative image of MCF10A$^{\text{AREG-MS2-KI}}$ cells co-expressing MCP-mNeon. Inset: A typical nascent transcription spot. (**c-h**) Mean transcriptional frequency before and after drug treatment. Transcriptional frequency was normalized to 1 for the 2-hr pre-treatment period. (**c**, **d**) Treatment with TG, mean+/-STD of three experiments for ANKRD1 (c) and AREG (d). (**e**, **f**) Pre-treatment with 1µM Go6976, followed by TG, mean+/-STD of three experiments for ANKRD1 (e) and AREG (f). (**g**, **h**) Treatment with 1uM PP1, mean+/-STD of 2 (ANKRD1) (g) and 3 (AREG) (h) experiments. (**i**) YAP localization (grey) in a dividing cell (condensed chromatin are shown in magenta). (**j, k**) Example of MCF10A$^{\text{AREG-MS2-KI}}$ (j) and MCF10A$^{\text{ANKRD1-MS2-KI}}$ (k) cells going through mitosis. Insets show nascent transcription spots in both daughter cells. (**l, m**) *Left axis:* Mean transcription frequency of cells showing transcription reset after mitosis for ANKRD1 (l) and AREG (m). Mitotic events collected from two independent experiments for both ANKRD1 (N=39 divisions) and AREG (N=25 divisions). *Right axis:* mean YAP N/C during division (N=24 divisions). The N/C ratio during mitosis was calculated as the mean value from 7 high-magnification images of mitotic cells expressing YAP (as shown in i).

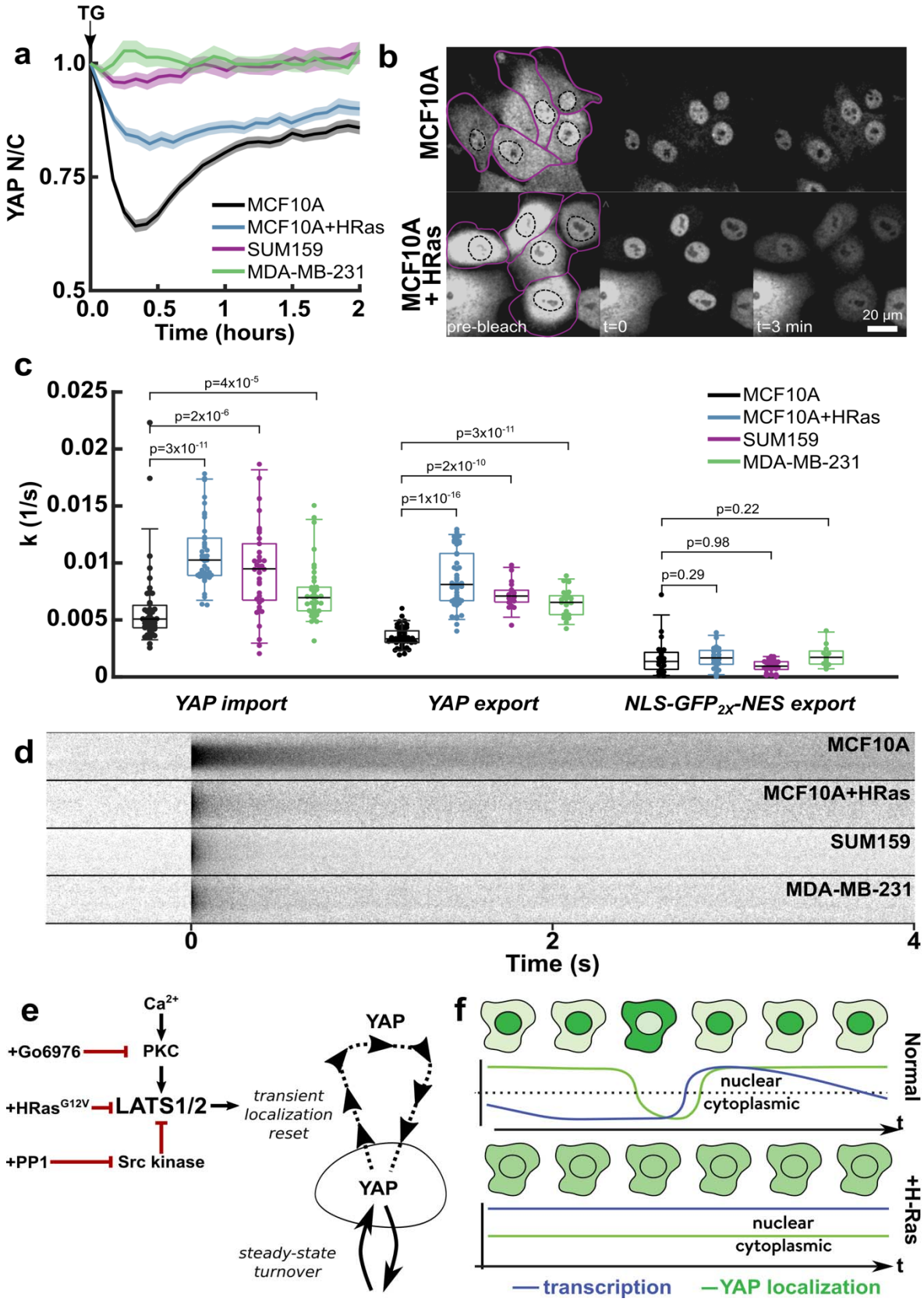
a
TG
YAP N/C
1.0
0.75
0.5
0.0
0.5
1
1.5
2
Time (hours)
MCF10A
MCF10A+HRas
SUM159
MDA-MB-231
b
MCF10A
MCF10A + HRas
pre-bleach
t=0
t=3 min
20 µm
c
k (1/s)
0.025
0.02
0.015
0.01
0.005
0
p=4x10-5
p=2x10-6
p=3x10-11
p=3x10-11
p=2x10-10
p=1x10-16
p=0.22
p=0.98
p=0.29
MCF10A
MCF10A+HRas
SUM159
MDA-MB-231
YAP import
YAP export
NLS-GFP2X-NES export
d
MCF10A
MCF10A+HRas
SUM159
MDA-MB-231
0
2
4
Time (s)
e
Ca2+
PKC
+Go6976
+HRasG12V
LATS1/2
+PP1
Src kinase
transient localization reset
YAP
YAP
steady-state turnover
f
Normal
nuclear
cytoplasmic
t
+H-Ras
nuclear
cytoplasmic
t
transcription
YAP localization

Figure 5: Ras transformation alters YAP dynamics. (**a**) Mean YAP N/C after TG treatment for MCF10A (N=157 tracks), MCF10A + HRas (N=75 tracks), SUM159 (N=70 tracks), MDA-MB-231 (N=101 tracks). (**b**) Representative images of FRAP experiments where cytoplasmic pool of YAP-eGFP is bleached and the nuclear pool is tracked over time. Nuclear boundaries are drawn with dashed black line while cytoplasm boundaries are drawn with solid purple line. HRas transformed cells show significant re-distribution by 3 minutes compared to MCF10A control. (**c**) Distribution of specific import and export rates of YAP, and the export rate of NLS-eGFP2x-NES for MCF10A (N YAP-imp=43, N YAP-exp=49, N exp=21), MCF10A + HRas (N YAP-imp=41, N YAP-exp=46, N exp=21), SUM159 (N YAP-imp=38, N YAP-exp=19, N exp=27), and MDA-MB-231 (N YAP-imp=38, N YAP-exp=23, Nexp=12) YAP-GFP knockin cell lines. P-values are calculated from one-sided Mann-Whitley U-test.
(**d**) Carpet plot generated from the average line FRAP of YAP-eGFP in various cell lines. (**e**) Summary of induction and modulation of transient YAP localization resets through LATS kinase. (**f**) Proposed model for the relationship between YAP dynamics and YAP responsive transcription.